Generation of Multiple Pharmacophore Hypotheses Using Multiobjective Optimisation Techniques

Simon J. Cottrell[1], Valerie J. Gillet[1*], Robin Taylor[2], David J. Wilton[1]

[1]Department of Information Studies, University of Sheffield, Regent Court, 211 Portobello Street, Sheffield S1 4DP, UK.

[2]Cambridge Crystallographic Data Centre, 12 Union Road, Cambridge, CB2 1EZ, UK

Keywords: pharmacophore identification, molecular overlay, alignment, evolutionary algorithms, MOGA, multiobjective optimisation, multiobjective genetic algorithm, conformational analysis

Summary

Pharmacophore methods provide a way of establishing a structure-activity relationship for a series of known active ligands. Often, there are several plausible hypotheses that could explain the same set of ligands and, in such cases, it is important that the chemist is presented with alternatives that can be tested with different synthetic compounds. Existing pharmacophore methods involve either generating an ensemble of conformers and considering each conformer of each ligand in turn or exploring conformational space on-the-fly. The ensemble methods tend to produce a large number of hypotheses and require considerable effort to analyse the results, whereas methods that vary conformation on-the-fly typically generate a single solution that represents one possible hypothesis, even though several might exist. We describe a new method for generating multiple pharmacophore hypotheses with full conformational flexibility being explored on-the-fly. The method is based on multiobjective evolutionary algorithm techniques and is designed to search for an

* To whom correspondence should be addressed. E-mail v.gillet@sheffield.ac.uk; Fax +44 1142 780 300

ensemble of diverse yet plausible overlays which can then be presented to the chemist for further investigation.

Introduction

A pharmacophore is the three-dimensional arrangement of functional groups required for activity. Pharmacophore methods are generally used in an attempt to establish a structure-activity relationship for a series of known active ligands in the absence of the three-dimensional structure of the target protein binding site. Thus, a pharmacophore hypothesis can be used to infer the characteristics of the binding site. Given a set of active molecules, pharmacophore methods involve analysing the molecules to identify pharmacophoric features (atoms or functional groups that can potentially interact with atoms in the binding site) and then aligning the active conformations of the molecules such that their corresponding pharmacophoric features are overlaid. A recent review on alignment methods is provided by Lemmen and Lengauer [1] and reviews on pharmacophore methods can be found in references [2-4].

There are two major issues to consider when generating pharmacophore hypotheses. First, most molecules can adopt more than one low-energy conformation and in many cases the number of accessible structures is very large. Thus, it can be very difficult to identify the active conformations of the molecules. Second, there can be several different pharmacophoric features within each molecule so that there can be many different ways of combining groups from different molecules. In general, the aim is to identify the pharmacophore(s) with the maximum number of pharmacophoric features, which must be presented by each molecule in a low-energy conformation.

Often, there are several plausible hypotheses that could explain the same set of molecules. In the absence of an experimental structure of the binding site it may not be possible to

distinguish between them. For example, it is frequently impossible to optimise the fit of the pharmacophoric features in each molecule to the pharmacophore points while at the same time minimising the conformational energy of each molecule. Thus, there can be different alternative compromise hypotheses. Even when considering fixed conformations, there may be different ways of aligning the molecules that are equally plausible. In such cases, it is important that the chemist is presented with alternative overlays that can be subsequently tested using different synthetic compounds.

When overlaying flexible molecules, it is necessary to perform conformational analysis, given that the active conformations are unknown a priori. There are two main approaches to this. One is to generate an ensemble of conformers and to consider each conformer of each ligand in turn for the alignment. This is the approach used in the commercially available programs Catalyst/HipHop [5, 6] and DISCO [7]. Ensemble methods tend to produce a large number of hypotheses and require considerable effort to analyse the results [8]. Furthermore, the results are dependent on the extent to which conformational space is sampled and on the structure generation method used.

An alternative approach is to explore conformational space on-the-fly, that is, at the same time as the alignment. This is the approach taken in GASP [9] which is based on a genetic algorithm that aims to optimise conformation simultaneously with the goodness of the alignment. Methods that vary conformation on-the-fly typically generate a single solution that represents one possible hypothesis, even though several might exist. For example, GASP attempts to find an optimum alignment that is based on a fitness function comprising three different objectives. These are: a similarity score, known as the feature score, which is based on the number of features in the pharmacophore and the goodness of the overlay, i.e. the degree to which the feature alignments are optimal; the van der Waals energy of the

individual conformers; and the volume integral of the overlay. The objectives are combined into a single function using a weighted-sum fitness function and the aim is to find the solution that maximises the function.

A difficulty with this approach is that the objectives are typically in competition. For example, Figure 1 illustrates two different (not particularly good) overlays of the three 5-HT_{1D} agonists shown in Figure 2. The solution on the left has a relatively high feature score but this is achieved by distorting the geometries of the molecules away from their minimum energy conformations. The solution on the right is more favourable in terms of energy but has a poorer feature score. In the absence of further information both solutions are equally plausible: they simply represent different compromises in the objectives. Thus a trade-off surface exists as illustrated schematically in Figure 3. The trade-off in two objectives only is shown, namely the feature score and energy, and the axes are arranged such that the best value for each objective is towards the origin. The two examples described occupy different relative positions on the trade-off surface with the surface itself representing all possible trade-off solutions. The trade-off surface is also known as the Pareto surface [10]. Combining the different objectives into a single weighted-sum fitness function effectively defines their relative importance and hence determines which particular compromise solution is found. The default weights assigned in GASP have been chosen empirically based on a small number of datasets and it is highly unlikely that they are optimal for all datasets. The appropriate set of weights for overlaying any given set of molecules is therefore unknown a priori.

In order to explore a range of possible hypotheses, GASP can be run a number of times and the best result from each run evaluated. However, the experiments reported later show that while carrying out multiple runs of GASP does generate a set of solutions, several of them

are typically suboptimal in terms of the fitness function (i.e., the GA has not converged). More importantly, the solutions are usually not distinct from one another in terms of the pharmacophores they represent.

Here, we describe a new method for generating multiple pharmacophore hypotheses with full conformational flexibility being explored on-the-fly. The method is based on multiobjective evolutionary algorithm (MOEA) techniques and Pareto ranking [10] and aims to generate a manageable number of different, yet plausible, hypotheses. Multiple solutions are explored in a single run, thus allowing cooperation between the solutions that are generated. The algorithm is designed to ensure that a diverse family of solutions is found.

To our knowledge, the first use of Pareto ranking in chemoinformatics is the work of Handschuh et al. [11] who used Pareto optimisation in their GA for the flexible superposition of 3D structures. Their method finds a set of common substructures between two molecules, based on two criteria: the number of atoms in the substructure and the fit of the matching atoms. These are conflicting criteria since a substructure which is a superstructure of a smaller substructure will tend to have a larger deviation in the coordinates of the superimposed atoms. Rather than attempting to combine the different criteria into a single weighted-sum fitness function, a set of Pareto-optimal solutions is obtained whereby an optimal geometric fit is found for each possible size of common substructure. While this approach is clearly related to the work described here, there are significant differences in the way in which the Pareto-optimal sets are identified. In the work of Handschuh et al., a finite set of solutions exists, with one solution for each size of common substructure. In our work, the continuous nature of the objectives being optimised (conformational energy, the volume score and the feature score) means that an infinite number of solutions exists and, as will be seen, identifying a useful subset of solutions has been a major challenge.

Since the work of Handschuh et al., Pareto ranking has been successfully applied to combinatorial library design [12, 13] where there is a requirement for libraries to be optimal over a number of conflicting properties; for example, they should be simultaneously diverse, cheap to synthesis and comprise of compounds with drug-like properties. It has also been applied to the derivation of quantitative structure-activity relationships [14] where model accuracy often conflicts with model complexity. More recently, Pareto ranking has been used for the evolution of median molecules [15].

Method

In a multiobjective evolutionary algorithm, the objectives to be optimised are treated independently. The concept of Pareto dominance is used to evolve a family of trade-off solutions in a single execution of the algorithm. In Pareto dominance, one solution dominates another if it is equal or better in all objectives, and strictly, it is better in at least one objective. A solution is classified as *non-dominated* or *Pareto optimal*, if no solution exists in the current population that dominates it. Thus, there are no solutions that are superior to a non-dominated solution, although there may be other equally good solutions. The set of all non-dominated solutions is known as the Pareto optimal set and the corresponding objective vectors are described as the Pareto front or the trade-off surface. The globally optimal trade-off surface of a multiobjective problem can contain a potentially infinite number of Pareto optimal solutions, and the task is usually to provide an accurate and useful representation of the trade-off surface. Thus, the solutions should have objectives values that are close to the true Pareto front; there should be good diversity in the solutions; and the solutions should be limited to pertinent regions of the search space (for example, pharmacophore solutions that involve molecules with very high conformational strain may not be relevant).

In this paper, we are concerned with exploring the benefits to be gained from the use of a true multiobjective optimisation method for pharmacophore identification over the more traditional GA. The main difference between a MOEA and a traditional evolutionary algorithm, such as a GA, is the way in which the fitness of an individual within the population is calculated. Thus, while many of the features of our algorithm are based on methods developed for GASP, there are significant differences in the way in which the objectives are handled. This is necessary to ensure that a family of equivalent solutions is found and considerable effort has been directed towards ensuring that the solutions found consist of diverse and relevant pharmacophore hypotheses.

The input, as with GASP, is the set of molecules to be overlaid, usually presented as energy-minimised conformers. The pharmacophoric features within each molecule are identified and virtual points created from them. Specifically, a virtual point is created at the centre of each aromatic ring and at 2.9Å from the heavy atom attached to each hydrogen-bond donor proton and each acceptor lone pair (to represent acceptor and donor atoms in the binding site, respectively). The molecule that contains the fewest features is then chosen as the base molecule onto which the other molecules are overlaid. As in GASP, the chromosome structure encodes the conformation of each molecule together with a mapping onto the base molecule of each molecule other than the base molecule itself. A molecular overlay consisting of N molecules therefore comprises $2N$-1 strings: N strings to encode the conformational information and N-1 strings to encode the mappings.

The first step of the fitness evaluation is to generate the alignment encoded in a chromosome. A conformation for each of the molecules is generated by applying the rotations encoded in the chromosome. Each molecule is then aligned to the base molecule according to the mapping encoded in the chromosome. The transformation is calculated to minimise the least-

squares distance between all the virtual points in the base molecule and the corresponding virtual points in the other molecules, as encoded in the mapping.

Once an alignment has been generated, the energy, volume integral and feature scores are calculated as in GASP [9]. The energy score is the mean internal van der Waals energy of the molecules. The volume integral score is the sum of the volume overlap integrals between the base molecule and each of the remaining molecules. The feature score is summed over all pharmacophore points. Two centroids are calculated for each mapping specified in the chromosomes; one for the virtual points and one for the corresponding heavy atoms. Distance thresholds are applied to determine if the mapping represents a valid pharmacophore point. If the mapping is valid, a contribution to the feature score is calculated based on the RMSD between the virtual points and their corresponding centroid and between the heavy atoms and their corresponding threshold.

Now, instead of summing the objective values into a single fitness value, as in GASP, the population is ranked using Pareto ranking as described by Fonseca and Fleming [10] in their Multiobjective Genetic Algorithm (MOGA). In MOGA, the rank of an individual is the number of individuals in the current population by which it is dominated. Thus, non-dominated individuals are assigned the rank 0, an individual that is dominated by one other individual is given rank 1, and so on. The rank value of an individual is then mapped to its fitness value. The subsequent roulette-wheel parent selection method then biases selection towards individuals with lower fitness values. By ensuring that all individuals at the same fitness have equal chance of being selected, the MOGA evolves the population towards the globally optimal Pareto surface. At the end of the run, the set of non-dominated solutions represents the Pareto surface and, ideally, all would be global optimal solutions with each one representing a different trade-off in the objectives.

Generating a Diverse Subset of Solutions

MOEAs have a tendency to converge to a restricted region of the Pareto surface so that not all of the search space is explored ("genetic drift"). This effect can be countered by implementing niching techniques that attempt to preserve the diversity of non-dominated solutions. Diversity can be a function of the objective values (objective-space niching) or the decision variables (decision-space niching). Objective-space niching is used to prevent the co-occurrence of solutions that differ only slightly in their objective values and can be used to ensure that solutions are evenly spread across the Pareto surface. Thus, objective-space niching could be used to ensure that the two 5-HT_{1D} agonist hypotheses identified earlier, which occupy distant points on the surface, are found (Figure 3). Initial attempts at preserving diversity were based on objective-space niching and were implemented using a sharing method [16] where the fitness values of individuals that lie within a given distance of one another (niche radius) are reduced in order to encourage the population to diverge from the niche. The sharing method involves modifying the fitness of each solution by an amount that is proportional to the number and distance of other solutions that lie within the niche radius. Distance was measured using Euclidean distance in objective space and the niche radius was defined independently for each objective, as shown in Table 1.

Initial results showed that while this method of niching was successful in spreading the solutions across the Pareto surface, it did not consistently result in the generation of chemically distinct overlays. Further investigation indicated that the lack of effectiveness was due to the weak correspondence between distance in objective space and distance in decision space. The two hypotheses illustrated in Figure 3 are distant in both objective and decision space, i.e. have different objective values and are chemically very different overlays. However, it is quite possible that solutions representing different overlays happen to have similar objective scores. For example, a small change in conformation may result in only a

small change in energy but may lead to a different atom in one molecule being matched to a given pharmacophoric feature in the base molecule. This would result in little change in the objective values, yet the solution represents a chemically different overlay. Conversely, it is also possible for solutions that represent similar overlays to be widely separated in objective space. For example, a small change in conformation may lead to a large change in energy without any significant change to the overlay. Figures 4 and 5 illustrate examples of both scenarios for the 5-HT_{1D} agonists.

The niching strategy was therefore modified to take account of decision-, or pharmacophore-space, in order to identify a subset of solutions that represent distinct, yet reasonable, hypotheses. In this method, the population is clustered into groups of similar pharmacophores prior to performing objective-space niching. A leader clustering method is used in which the first pharmacophore encountered defines a cluster. If the next pharmacophore represents a mapping that is distinct from the first it is assigned to a new cluster, otherwise it is assigned to the same cluster as the first. Two pharmacophores represent distinct mappings when either of the following occurs:

- Different sets of base molecule features are mapped.
- The same set of base molecule features are mapped, but at least one feature maps to a different feature in at least one molecule.

The definition of a cluster is extended to include pharmacophores that are subsets of other pharmacophores, i.e., that consist of a subset of the points contained in the other. In this case, the smaller pharmacophore is assigned to the same cluster as its parent. An individual may be a subset of more than one parent pharmacophore, in which case, its membership is shared between clusters.

The fitness values of individuals are then modified from their initial values (which correspond to their Pareto ranks) to differentiate solutions of the same Pareto rank according to cluster density. Thus, the probability of selecting an individual is adjusted by an amount that is inversely proportional to the density of the cluster to which it belongs. For example, the fitness of a non-dominated solution that belongs to a cluster containing four solutions is adjusted so that there is half the probability of it being selected compared to a non-dominated solution that belongs to a cluster containing two solutions. The probability of selecting a solution with a low rank is still greater than the probability of selecting one at higher rank, but within a given rank the probability of selecting a solution from a sparsely populated cluster is greater than the probability of selecting one from a more dense cluster.

Finally, objective-space niching is applied to solutions within the same cluster, with the fitness of an individual being further modified according to the number of individuals which lie within its niche-radius and which belong to the same cluster. The overall probability of selecting a solution from each cluster is unaffected. Restricting objective-space niching to within a cluster means that solutions that are close on the Pareto surface are only penalised if they represent the same mapping. Thus, the primary aim of the niching is to preserve diversity in terms of the number of different pharmacophore mappings, or clusters, that exist in the population, with the secondary aim being to ensure diverse coverage of the Pareto surface within a cluster, as defined by the objectives.

A threshold value is placed on the energy objective to ensure that solutions are limited to pertinent regions of the search space. In pharmacophore generation, highly strained conformers are generally not of interest and the threshold (21000 kJ mol^{-1}) is used to exclude individuals that have energies that exceed this value. The energy threshold is set to a high value because valence angles are not allowed to change when conformations are generated.

Thus, molecules do not have the ability to relieve short non-covalent contacts by minor valence-angle distortions. No limits are placed on the feature or volume scores since it is necessary to allow individuals with low values of these scores to exist in the population, especially early in the search, and because these objectives have finite lower bounds.

Results and Discussion

Datasets

Results are presented for three datasets: the three 5-HT_{1D} agonists, shown in Figure 2; a set of four scytalone dehydratase inhibitors, Figure 9; and a set of three dopamine D_2 antagonists shown in Figure 13. For each dataset, the solutions found in a single run of the MOGA are compared with those found by running GASP ten times. This approach allows a direct comparison to be made between the multiobjective optimisation approach used in the MOGA and the traditional weighted-sum approach used in GASP.

As discussed in the methodology, the MOGA solutions are clustered such that all solutions within a cluster consist of the same pharmacophoric features, with the same mapping from each molecule to the features. While solutions within a cluster will have different values of the objectives (for example, the conformations of the molecules may be different and the feature scores may vary, so that the solutions are separated on the Pareto surface) the basic pharmacophore is the same. A representative solution from each cluster is shown in the results and solutions with fewer than three pharmacophoric features have been omitted. Where possible, a non-dominated solution is chosen as cluster representative, however, dominated solutions are chosen to represent clusters which do not contain any non-dominated solutions. The non-dominated solutions represent globally optimal solutions and are clearly solutions of interest. However, the dominated solutions may also represent plausible hypotheses even though there are other solutions with improved scores over each of the

objectives. This is due to the fundamental limitation of pharmacophore methods whereby the contribution of the receptor cannot be modelled and the objectives being optimised are based on the ligands only.

MOGA and GASP Parameters

The search space explored by a MOGA is considerably larger than that explored by a traditional GA, since it attempts to find multiple diverse solutions spanning the entire Pareto surface. In contrast, a GA attempts to find a single solution only. Thus, a MOGA requires a bigger population size to ensure adequate coverage of the search space. Unless otherwise stated, the runs reported here used the parameters as specified in Table 1. The run times for 200000 iterations are approximately 2 hours on a Linux PC running at 2.8GHz. GASP was run using the default weights and with parameters as shown in Table 1.

5-HT_{1D} agonists.

The exact structure of the 5-HT_{1D} receptor is not known; however, Glen et al. have produced a 3D pharmacophore hypothesis using the active analogue approach [17]. Molecules **1**–**3** in Figure 2 form part of the much larger dataset used in that study. As methysergide (**3**) is relatively inflexible, it was used by Glen et al. as a scaffold to which more flexible molecules could be fitted. A pharmacophore hypothesis was generated involving five features; in methysergide, these are:

- the aromatic ring
- the protonated amine (as a donor)
- the amide oxygen (as an acceptor)
- the hydrophobic region comprising the ethyl group

- the hydroxyl oxygen (as an acceptor)

The last two features are not essential: active molecules have been found that do not contain them, such as **1** and **2**, though their absence generally lowers affinity for the 5-HT_{1D} receptor. According to Glen et al.'s hypothesis, the aromatic rings and the protonated amine hydrogens in **1**, **2** and **3** are mapped to each other, and the amide oxygen of **3** is mapped to the carbonyl oxygen of **1** and one of the sulphonamide oxygens of **2**.

Five different, reasonably plausible ways of aligning the molecules are shown in Figure 6. The alignments vary in the pharmacophoric features identified and the features in the individual molecules that map to the pharmacophore. The variations arise from small changes either in the relative position of one or more of the molecules or in the conformations of the molecules. The hypothesis identified by Glen et al. corresponds to alignment 3 in Figure 6, although in the figure it is the hydroxyl oxygen rather than the amide oxygen of **3** that is mapped.

The results for the ten GASP runs are shown in Table 2, which indicates the features of methysergide, **3**, that are mapped to pharmacophoric points (the features of molecules **1** and **2** that map to the pharmacophore are not indicated). Energy is reported relative to the energy of the input molecules. All solutions correspond to the general alignment 3 shown in Figure 6. The fittest solution contains the three features identified as important by Glen et al., but it also includes another feature generated from the overlay of the amide/sulphonamide hydrogens. Furthermore, the conformation of **3** is considerably different to that reported by Glen et al., with the distorted conformation allowing the additional pharmacophoric feature to be identified. Therefore, the "best" GASP solution does not represent the pharmacophore derived by Glen et al. In fact, there are no solutions from the ten runs that correspond exactly to this pharmacophore model.

Figure 7a shows the objective values of the ten GASP solutions as a parallel coordinates graph. The objectives are plotted along the x-axis and the values of the objectives are plotted along the y-axis, linearly scaled so that the best value achieved for each objective is at 0 and the worst is at 1. Each solution is represented as a continuous line. The plot gives an indication of the variation found when performing multiple runs of GASP. Crossing lines in the plot indicate solutions that represent different compromises in the objectives whereas lines that do not cross indicate the presence of dominated solutions. Thus, solutions 2 and 9 are both relatively good in terms of energy and features but they have relatively poor volume overlays. Conversely, solutions 3, 4, 6 and 8 are good in terms of volume and energy but are relatively poor in terms of their feature scores. Solution 5 is poor in all objectives. In a Pareto sense, it is dominated by all the others except solution 9 (only solution 9 crosses it in the graph), which may indicate that this run of GASP did not reach convergence. If all dominated solutions are removed, only 5 of the 10 solutions remain, as shown in Figure 7b.

Table 3 shows the results for four runs of the MOGA. As for the GASP results, the pharmacophoric features are indicated with reference to methysergide. In addition, the solutions are labelled according to the alignment to which they are closest. Where a solution cannot be clearly assigned to one of the five alignments in Figure 6, the alignments that it shares characteristics with are indicated. Thus, it can be seen that each of the MOGA runs generates solutions that correspond to several of the alignments of Figure 6 and, considering all of the MOGA runs together, all five distinct alignments are found.

The solution shown in bold corresponds exactly to the pharmacophore suggested by Glen et al. in terms of the pharmacophoric features identified and the inter-feature distances, which fall within the range specified by those workers (Figure 8). However, the conformation of methysergide differs from the conformation illustrated in Glen et al. Comparing the objective

values of this solution with those found by GASP shows that the GASP runs have a tendency to promote the feature score over the other objectives, as seen by the relatively small range of values for this score found over the multiple runs. The MOGA solution has a lower features score than any of the GASP solutions and therefore it is unlikely that it would be found using the default GASP weights.

The ability of the MOGA to map out the Pareto surface is shown by the greater range of feature scores seen in the solutions found in a single run. The greater range of hypotheses generated clearly demonstrates the advantages of using the MOGA over GASP. However, there is a lack of consistency between MOGA runs. Increasing the population size to 2000 results in greater consistency in the ranges of the values of the objectives that are seen in each run. However, considerable extra computational resource is required; these runs take around 11 hours to complete, compared to two to three hours per run with a population of 1000.

Scytalone dehydratase inhibitors.

The scytalone dehydratase inhibitors were extracted from enzyme-inhibitor complexes in the Protein Data Bank (PDB) [18]. Therefore, the bound conformations of the inhibitors are known. Since **4**–**6** have a large common substructure (consisting of the amide and the aromatic ring to which the chlorine or bromine is attached), it seems likely that these common features will form the same interactions with the enzyme. However, the interactions of **7** are less obvious. The four aromatic rings of **7** have been labelled for reference purposes. From inspection, overlays with each of the four rings mapped to the aromatic ring of **4** (the base molecule) seem plausible; example overlays are shown in Figure 10. Comparison of the crystal structures indicates that it is actually ring 3 of **7** that maps to the aromatic ring of **4**. An alignment has been generated using the crystal structures (Figure 11). The flexibility of

the protein is such that it is not possible to align the complexes exactly and hence the alignment generated is somewhat arbitrary.

The GASP results are shown in Table 4 with the different alignments labelled according to the ring of **7** that is mapped to the aromatic ring of **4**. Three out of the four alignments are generated. However, only one of the runs produces the correct alignment and this solution is the one with lowest overall fitness score, i.e., at rank ten when the solutions are ranked on fitness. This solution has a relatively low score and is dominated by all of the other solutions except for solution nine, which is worse in energy. Thus, although this solution represents the correct overlay, it occupies a local maximum in the search space and has been found as a result of GASP's failure to move towards the global maximum in this particular execution of the program.

A run of the MOGA finds examples of all the overlays shown in Figure 10 (Table 5; the ring of **7** that is mapped to the aromatic rings of the other molecules is indicated). As for the 5-HT_{1D} dataset, considerable variation is seen over all of the objectives, indicating that the Pareto surface has been explored to a reasonable degree. The negative energy scores are due to the generation of conformations that are lower in energy than the starting conformations. The MOGA finds two solutions with the correct alignment. One of these is better than the GASP alignment in all objectives, i.e. this solution would dominate the "correct" GASP solution. An additional feature is seen in this solution relative to the manually derived solution, both lone-pairs of the carbonyl groups in **4**-**6** giving rise to acceptor points. The other solution has poorer feature and energy scores but the overlay has an improved volume integral. In both cases, the geometry of the pharmacophore fits the manually generated pharmacophore very accurately (RMSD 0.27Å and 0.21Å respectively). However, in both

cases the benzene ring of **7** is in a different position to that observed in the crystal structure. These two solutions are shown in Figure 12.

A second run of the MOGA also produced examples of all four alignments, although some variation was seen in the individual objective values. Increasing the population size to 2000 resulted in all of the alignments seen previously, together with an increased number of less plausible solutions. Therefore, a population size of 1000 would appear to be adequate in this case.

Dopamine D_2 antagonists.

All three molecules in the dopamine dataset are very flexible and feature rich [19]. This makes the dataset difficult for any pharmacophore generation method since there are many different ways in which the molecules could reasonably be overlaid.

Although the dopamine D_2 receptor has been studied in detail, we are unaware of a published pharmacophore hypothesis for exactly the three molecules in our dataset. However, a receptor-interaction model has been published by Liljefors and Bøgesø [20], and close analogues of **8** and **10** were fitted to this model by Pettersson and Liljefors [21]. The essential features of this model are the aromatic ring and the protonated amine.

The dopamine D_4 receptor is very similar to the D_2 receptor, and a pharmacophore model for the D_4 receptor has also been published [22]. The only difference from the D_2 pharmacophore is that the D_4 model includes two receptor-essential volumes that are not part of the D_2 model. Compound **9** has been fitted to the D_4 model in a way that implies a mapping between the fluorobenzene ring of **9** and the benzene rings of **8** and **10**, and between the protonated amines of all three molecules. The chlorobenzene ring of **9** is also believed to be significant

to its activity, but as there are no equivalent features in **8** and **10**, this feature will not be found by either method.

In the absence of knowledge of these studies, compound **9** could reasonably be aligned either in the orientation described above, or it could be flipped completely such the fluorobenzene ring is aligned towards the pyrrolidinium rings in **8** and **10**. Even within each of these general alignments, considerable variation is possible both in conformations and the relative positions of the molecules. This leads to many different potential pharmacophores.

The results for the ten GASP runs are shown in Table 6. Six of the ten solutions represent alignments where the fluorobenzene ring of **9** aligns to the benzene rings of **8** and **10**, indicated by a tick in the column headed R_F. The other four solutions have **8** oriented in the opposite direction (indicated by a tick in the column headed R_{CL}). However, none of the solutions corresponds exactly to the pharmacophore model described above. Comparing the objective scores across the runs shows that four of the solutions represent non-dominated solutions (solutions 1, 2 , 4 and 8 are non-dominated).

The solutions found in a single run of the MOGA are shown in Table 7 and also include several examples of both alignments of **9**. However, a greater range of values is seen in all the objectives, with a significant number of solutions with lower energies than is found in the GASP runs. Solutions with higher volume overlays are also seen. As for the previous datasets, the MOGA shows a bias towards solutions with favourable energies and volume scores relative to the feature scores. Figure 14 shown a diverse set of alignments as found by the MOGA.

In this case, the large search space is such that it is unlikely that GASP will generate the same solution in different runs. Hence, it could be argued that the MOGA offers no advantage, since multiple runs of GASP will generate diverse solutions. However, in GASP there is no

cooperation between distinct runs, so the identification of diverse solutions is left to chance. Furthermore, the generation of a wide range of diverse solutions with GASP is likely to require repeated runs where the relative weights of the objectives are varied. With the MOGA, multiple solutions are sought within the same exploration of the search space and the search is explicitly directed towards a diverse set of solutions.

Conclusions

It is rarely possible to overlay unambiguously a set of molecules known to bind at the same protein binding site. Usually, pharmacophoric features in the different molecules may be matched in several ways, and, unless some of the molecules are rigid, the molecules may be superimposed in various conformations. Thus, it is important that a range of different, plausible overlays (i.e. structure-activity hypotheses) is identified and presented to the chemist for browsing and visual inspection. It is then possible for the chemist to design synthetic targets or pharmacophore searches that will test, and therefore confirm or eliminate, the more likely-looking hypotheses. Pharmacophore generation programs like GASP aim to produce a single hypothesis which optimises a reasonable, but essentially arbitrary, linear combination of objective functions. Repeated runs of GASP may, in fact, produce different overlays. When this occurs, however, it merely indicates that the search algorithm is unreliable at finding the global optimum; it is not a satisfactory way of searching for a diverse range of feasible overlays.

In contrast, the MOGA described above looks for a representative ensemble of overlays in a concerted fashion. Our results show that a single run of the MOGA tends to find a wider range of overlay hypotheses than repeated runs of GASP. In particular, the weighting scheme in GASP clearly emphasises the feature-score term (goodness-of-fit to pharmacophore points) at the expense of volume integral and strain energy. In at least one case (5-HT_{1D} agonists),

this makes it difficult if not impossible for GASP to find the pharmacophore hypothesis proposed in the literature. Even with the MOGA, however, we find that repeated runs will sometimes find different solutions, especially when relatively small population sizes are used. This is a reflection of the complexity of the search space and the small datasets we have used. In particular, we must expect any search algorithm to be unstable when applied to the three highly flexible and feature-rich dopamine antagonists **8**-**10**. Even in this situation, however, it is better for the chemist to be presented with a large and unbiased range of credible solutions than a small arbitrary subset that is ultimately dependent on the particular weighting scheme used in GASP.

The programs Catalyst and DISCO, described earlier, are both designed to generate multiple pharmacophore hypotheses. However, a fundamental difference between these programs and the MOGA (and also GASP) is that both Catalyst and DISCO require a precomputed set of conformers for each of the ligands. They then use rigid body alignment techniques which are applied to each conformer of each ligand in turn. As a consequence, the pharmacophores that are generated by these methods are highly dependent on the structure generation method that is used [23]. The MOGA allows a more complete exploration of conformational space and is not limited to finding conformational minima. A further major strength of the MOGA is that the steric overlay of the ligand is taken into account so that most of the alignments that are generated seem sensible. Catalyst, on the other hand, does not taken account of steric overlap and as a result a large number of the alignments can be generated that appear unlikely.

A difficulty in assessing the performance of any pharmacophore generation method is that the correct answer is usually unknown. In previous work, we compared the performance of GASP with Catalyst and DISCO in generating pharmacophores for sets of ligands whose binding modes have been determined experimentally, so that the true pharmacophore is

known [8]. This work highlighted a significant limitation of GASP that has not been addressed here, which is that GASP requires every molecule to match every feature in the pharmacophore. The same limitation applies to the MOGA. Current work is focussing on relaxing this constraint so that we can apply the method to larger datasets. Efforts are also underway to improve the stability of the MOGA so that less variation is seen from one run to another.

Acknowledgements

We acknowledge funding from EPSRC and Cambridge Crystallographic Data Centre, and software support from Tripos Inc.

References

1. Lemmen, C. and Lengauer T. J. Comput.-Aided Mol. Des., 14 (2000) 215.

2. Güner, O.F., (Ed.) Pharmacophore Perception, Development, and Use in Drug Design. International University Line, La Jolla, CA, 2000.

3. Dror, O., Shulman-Peleg, A., Nussinov, R. and Wolfson, H. J. Current Medicinal Chemistry, 11 (2004) 71.

4. van Drie, J.H. Current Pharmaceutical Design, 9 (2003) 1649.

5. Barnum, D., Greene, J., Smellie, A. and Sprague, P. J. Chem. Inf. Comput. Sci. 36 (1996) 563.

6. Smellie, A., Teig, S.L. and Towbin, P. J. Comp. Chem., 16 (1995) 171.

7. Martin, Y.C., Bures, M.G., Danaher, E.A., DeLazzer, J., Lico, I. And Pavlik, P.A. J. Comput. Aided Mol. Design, 7, (1993) 83.

8. Patel, Y., Gillet, V.J., Bravi, G. and Leach, A.R. J. Comput.-Aided Mol. Des., 16 (2002) 653.

9. Jones, G., Willett, P. and Glen, R.C. J. Comput.-Aided Mol. Des., 9 (1995) 532

10. Fonseca, C.M. and Fleming, P.J. IEEE Transactions on Systems Man and Cybernetics Part a-Systems and Humans, 28 (1998) 26.

11. Handschuh, S., Wagener, M. and Gasteiger, J. J. Chem. Inf. Comput. Sci. 38 (1998) 220.

12. Wright, T., Gillet, V. J., Green, D.V.S, and Pickett, S.D. J. Chem. Inf. Comput. Sci.. 43 (2003) 381.

13. Gillet, V.J., Khatib, W., Willett, P. Fleming, P.J., and Green, D.V.S. J. Chem. Inf. Comput. Sci.. 42 (2002) 375.

14. Nicolotti, O., Gillet, V.J., Fleming, P.J., and Green, D.V.S. J. Med. Chem. 45 (2002) 5069.

15. Brown, N., McKay B., Gilardoni, F. and Gasteiger, J. J. Chem. Inf. Comput. Sci.. 44 (2004) 1079.

16. Goldberg, D.E. and Richardson J. In Grefenstette, J.J. (Ed.) Genetic Algorithms with Sharing for Multimodal Function Optimisation, in Proceedings of the Second International Conference on Genetic Algorithms, Lawrence Erlbaum Associates, Hillsdale. 1987, pp. 41-49.

17. Glen, R.C., Hill, A.P., Martin, G.R. and Robertson, A.D. J. Med. Chem. 38 (1995) 3566.

18. Wawrzak, Z., Tatyana, S., Steffens, J.J., Basarab, G.S., Lundqvist, T., Lindqvist, Y. and Jordon, D.B. Proteins: Structure, Function and Genetics**,** 1999, 35 (1999), 425.

19. Höberg, T. and Norinder, U. In Krogsgaard-Larsen, P., Liljefors, T. and Madsen, U. (Eds.) A Textbook of Drug Design and Development, 2nd Edition, Harwood Academic Publishers, Amsterdam. 1996, pp. 94-130.

20. Liljefors, T. and Bøgesø, K.P. J. Med. Chem. 31 (1988) 306.

21. Pettersson, I. and Liljefors, T. J. Med. Chem. 35 (1992) 2355.

22. Boström, J., Gundertofte, K. and Liljefors, T. J. Comput.-Aided Mol. Des., 14 (2000) 769.

23. Kristam, R., Gillet, V.J., Lewis, R.A. and Thorner D. Submitted.

Figure Captions

Figure 1. The overlay on the left has the following objective values: feature score = 2.72 (representing 4 pharmacophore points) and energy = 247 kJ mol^{-1}. The overlay on the right has objective values: feature score = 1.22 (representing 2 pharmacophore points) and energy = 6 kJ mol^{-1}. Thus, the higher feature score is achieved at the expense of conformational energy. Donors are shown in purple; acceptors in pink; and hydrophobes in cyan. Molecule **1** is in white; molecule **2** in brown; and molecule **3** in blue (see Figure 2).

Figure 2. 5-HT_{1D} agonists.

Figure 3. Schematic of the position of the two overlays illustrated in Figure 1 on the Pareto surface. Two objectives only are shown for simplicity. Colour scheme as for Figure 1.

Figure 4. Similar overlays of the 5-HT_{1D} ligands that occupy distant points on the Pareto surface due to differences in their objective values. Overlay (a) has the following objective values: feature score = 1.61; volume overlay = 1184 $Å^3$ and conformational energy = 579 $kJmol^{-1}$. Overlay (b) has the following objective values: feature score = 0.72; volume overlay = 868 $Å^3$ and conformational energy = 5 $kJmol^{-1}$. Colour scheme as for Figure 1.

Figure 5. Different overlays of the 5-HT_{1D} ligands that have similar objective values and hence are close on the Pareto surface. Overlay (a) has the following objective values: feature score = 1.51; volume overlay = 1003 $Å^3$ and conformational energy = 99 $kJmol^{-1}$. Overlay (b) has the following objective values: feature score = 1.54; volume overlay = 983 $Å^3$ and conformational energy = 30 $kJmol^{-1}$. Colour scheme as for Figure 1.

Figure 6. Alignments of 5-HT_{1D} agonists. Colour scheme as for Figure 1.

Figure 7. (a) Parallel coordinates graph representation of the GASP solutions. (b) Five of the GASP solutions are non-dominated solutions.

Figure 8. The “correct” alignment generated by the MOGA. The figure on the left indicates the distances between the site points whereas the figure on the right indicates the distances corresponding to the positions of the heavy atoms. Colour scheme as for Figure 1.

Figure 9. Scytalone dehydratase inhibitors.

Figure 10. Different alignments for the scytalone dehydratase inhibitors with the different rings of **7** aligned to the benzene ring of **4**. Donors are shown in purple; acceptors in pink; and hydrophobes in cyan. Molecule **4** is in white; molecule **5** in orange; molecule **6** in blue; and molecule **7** in brown.

Figure 11. The manual pharmacophore for the scytalone dehydratase inhibitors generated by overlaying the crystal structures. Colour scheme as for Figure 10.

Figure 12. Two solutions generated by the MOGA that correspond to alignment 3. Colour scheme as for Figure 10.

Figure 13. Dopamine antagonists.

Figure 14. Alignments of dopamine D_2 antagonists. Donors are shown in purple; acceptors in pink; and hydrophobes in cyan. Molecule **8** is in brown; molecule **9** in white; and molecule **10** in blue.

Tables

MOGA Parameters	
Population size	1000
Selection pressure	1.05
No of operations	200000
Crossover rate	50%
Mutation rate	50%
Features niche radius	2
Volume overlap niche radius	100 $Å^3$
Energy niche radius	42 kJ mol^{-1}
GASP Parameters	
Population size	100
No. of subpopulations (islands)	5
Selection pressure	1.1
Crossover rate	47.5%
Mutation rate	47.5%
Migration rate	5%
Niche size	2
Energy weight*	0.05
Features weight	750
Volume weight	1 (by definition)
Convergence criteria	No increase in fitness > 0.01 over 6500 runs

*Note that the energies in GASP are in $kcal.mol^{-1}$

Table 1. The parameters used in the MOGA and GASP runs, respectively.

Run	Total	Energy	Volume	Feature	Ring	Amine (donor)	Carbonyl (acceptor)	Hydroxyl (acceptor)	Hydroxyl (donor)	Amide (donor)
2	3076.61	163.51	1065.80	2.68	**ü**	**ü**	**ü**			**ü**
4	3046.21	231.04	1191.61	2.48	**ü**	**ü**				**ü**
6	3045.07	319.16	1228.58	2.43	**ü**	**ü**			**ü**	
3	3027.16	236.21	1209.15	2.43	**ü**	**ü**			**ü**	
9	3020.25	177.53	1007.00	2.69	**ü**	**ü**		**ü (x2)**		
8	2972.20	442.05	1199.30	2.37	**ü**	**ü**				**ü**
1	2956.92	819.25	1182.92	2.38	**ü**	**ü**				
10	2926.20	1240.05	1043.94	2.53	**ü**	**ü**				**ü**
7	2843.63	297.15	1046.11	2.40	**ü**	**ü**	**ü**			**ü**
5	2708.31	1281.76	1023.30	2.27	**ü**	**ü**				**ü**

Table 2. GASP results for 5-HT_{1D} dataset. The runs are ordered on fitness value. The dominated solutions are shown as shaded. Energies in this and in all subsequent tables are given in kJ mol^{-1}.

Alignment	Energy	Volume	Feature	Ring	Amine (donor)	Carbonyl (acceptor)	Hydroxyl (acceptor)	Hydroxyl (donor)	Amide (donor)
					Run 1				
1	-0.25	699.39	1.08	**ü**		**ü**	**ü**		
1	1.22	653.60	0.58	**ü**		**ü (x2)**			
3	64.22	1018.77	2.22	**ü**	**ü**				**ü**
4	11.21	923.36	1.04			**ü (x2)**	**ü (x2)**		
					Run 2				
1	-3.40	1065.66	0.71		**ü**		**ü (x2)**		
3	2.14	1015.81	1.98	**ü**	**ü**			**ü**	
4	2.60	987.46	1.27	**ü**		**ü (x2)**			
5	242.68	982.73	1.54	**ü**	**ü**				**ü**
					Run 3				
1/3	7021.69	1085.97	1.92	**ü**	**ü**				**ü**
4	3.53	857.57	1.38	**ü**	**ü**		**ü (x2)**	**ü**	
					Run 4				
1	-3.40	900.17	1.04	**ü**		**ü**	**ü**		
1	2.14	829.55	1.39	**ü**		**ü (x2)**			
2	2.60	909.50	0.93	**ü**	**ü**				**ü**
3	242.68	1085.53	2.23	**ü**	**ü**		**ü**		
3	395.51	1115.69	2.17	**ü**	**ü**		**ü**		
3	2.23	903.63	1.54	**ü**	**ü**		**ü**		**ü**
3	**98.78**	**1003.41**	**1.51**	**ü**	**ü**	**ü**			
4	-5.80	483.07	0.65			**ü**	**ü**	**ü**	

Table 3. MOGA solutions found over four runs. The column headed Alignment indicates the alignment in Figure 6 that the solution corresponds to. The shaded rows indicate solutions that are dominated. The solution given in bold matches the solution found by Glen et al. exactly in terms of the features found and the distances between them.

Run	Alignment	Fitness	Energy	Volume	Features
5	1	2891.08	654.11	1079.46	2.43
3	2	2793.06	956.34	993.50	2.41
8	1	2792.55	1266.76	990.19	2.42
7	2	2684.94	95.55	986.19	2.27
6	1	2631.01	894.81	931.72	2.28
4	1	2587.76	106.64	957.32	2.18
2	2	2586.81	995.27	974.65	2.17
9	2	2538.65	1105.65	901.48	2.20
1	1	2526.47	3320.10	947.88	2.16
10	3	2309.28	2550.49	876.79	1.95

Table 4. GASP results for the scytalone dehydratase dataset. The column headed Alignment indicates the ring of **7** that is superimposed to the aromatic ring of **4**. The dominated solutions are shaded.

Alignment	Energy	Volume	Features
1	-4.91	897.98	0.82
1	11.17	978.07	0.84
2	28.60	838.82	1.78
2	94.00	1000.16	1.63
2	10.50	871.98	1.17
2	-20.12	638.56	0.32
3	45.11	989.68	2.09
3	65.31	1004.30	1.47
4	1311.83	1129.30	1.06
4	1106.99	1074.46	1.39
4	7.35	929.55	0.96
4	47.12	974.17	1.06
N	7.10	942.08	0.32
N	4.79	910.03	0.78

Table 5. MOGA results for the scytalone dehydratase dataset. The shaded rows represent dominated solutions. The column headed Alignment indicates the ring of **7** that is mapped to the benzene ring in **4**. An N indicates that none of the rings of **7** map to the ring in **4**.

Run	Fitness	Energy	Volume	Features	H_1	H_2	LP_1	LP_2	LP_3	LP_4	R_{Cl}	R_F
1	3073.45	572.92	1036.21	2.73		**ü**			**ü**	**ü**		**ü**
2	2918.41	329.66	1012.3	2.55		**ü**	**ü**	**ü**			**ü**	
5	2826.05	775.95	1006.95	2.44		**ü**			**ü**	**ü**		**ü**
7	2818.6	3129.42	968.88	2.52		**ü**			**ü**	**ü**		**ü**
3	2767.67	891.24	994.14	2.38	**ü**	**ü**	**ü**				**ü**	
8	2728.25	590.31	1050.68	2.25		**ü**						**ü**
4	2666.54	200.68	969.09	2.27		**ü**				**ü**		**ü**
10	2506.36	580.23	802.44	2.28		**ü**	**ü**	**ü**			**ü**	
9	2403.55	202.48	899.58	2.01		**ü**	**ü**	**ü**			**ü**	
6	2375.49	1404.31	903.16	1.99		**ü**						**ü**

Table 6. GASP results for the dopamine dataset sorted on fitness. The dominated solutions are shaded. A tick in the column headed R_F indicates that the fluorobenzene ring of compound **9** is aligned with the benzene rings in **8** and **10**, whereas a tick in the column headed R_{CL} indicates that compound **9** is flipped completely so that the chlorobenzene ring corresponds to the benzene rings.

Energy	Volume	Features	H_1	H_2	LP_1	LP_2	LP_3	LP_4	R_{Cl}	R_F
84.92	997.13	1.67				**ü**	**ü**	**ü**		**ü**
5704.65	1065.34	1.54			**ü**		**ü**	**ü**		**ü**
2975.15	1086.32	1.53			**ü**		**ü**	**ü**		**ü**
277.83	1068.03	1.50	**ü**				**ü**	**ü**		**ü**
-1.09	631.01	1.47	**ü**		**ü**	**ü**			**ü**	
4.79	754.47	1.44			**ü**	**ü**			**ü**	
-3.15	930.90	1.43	**ü**	**ü**				**ü**		**ü**
86.48	1054.33	1.40	**ü**					**ü**		**ü**
27.93	991.07	1.39	**ü**	**ü**			**ü**			**ü**
369.26	1163.89	1.37					**ü**	**ü**		**ü**
45.74	1044.92	1.33	**ü**					**ü**		**ü**
5.42	863.84	1.26		**ü**	**ü**				**ü**	
-6.85	809.11	1.06		**ü**		**ü**			**ü**	
-9.32	600.21	0.88		**ü**	**ü**	**ü**				
-8.44	657.50	0.83		**ü**			**ü**	**ü**		
-11.55	720.39	0.75		**ü**	**ü**	**ü**				
-7.94	719.69	0.75		**ü**	**ü**	**ü**				
-7.18	855.94	0.72		**ü**			**ü**	**ü**		
27.72	1123.71	0.69	**ü**	**ü**			**ü**			
-11.59	652.40	0.63		**ü**	**ü**	**ü**				
-11.59	578.60	0.63		**ü**	**ü**	**ü**				
-6.26	925.47	0.63	**ü**				**ü**	**ü**		
-11.59	767.75	0.55		**ü**	**ü**	**ü**				
-10.12	807.58	0.51		**ü**			**ü**	**ü**		
-11.63	509.94	0.50		**ü**	**ü**	**ü**				
-11.59	449.49	0.49		**ü**	**ü**	**ü**				
-10.84	796.63	0.45		**ü**	**ü**	**ü**				
-10.29	904.28	0.41		**ü**			**ü**	**ü**		
-11.59	658.77	0.40		**ü**	**ü**	**ü**				

Table 7. MOGA solutions for the dopamine dataset. The solutions are ordered on decreasing feature score. The shaded rows represent dominated solutions. The final two columns indicate the orientation of **9** relative to **8** and **10**.

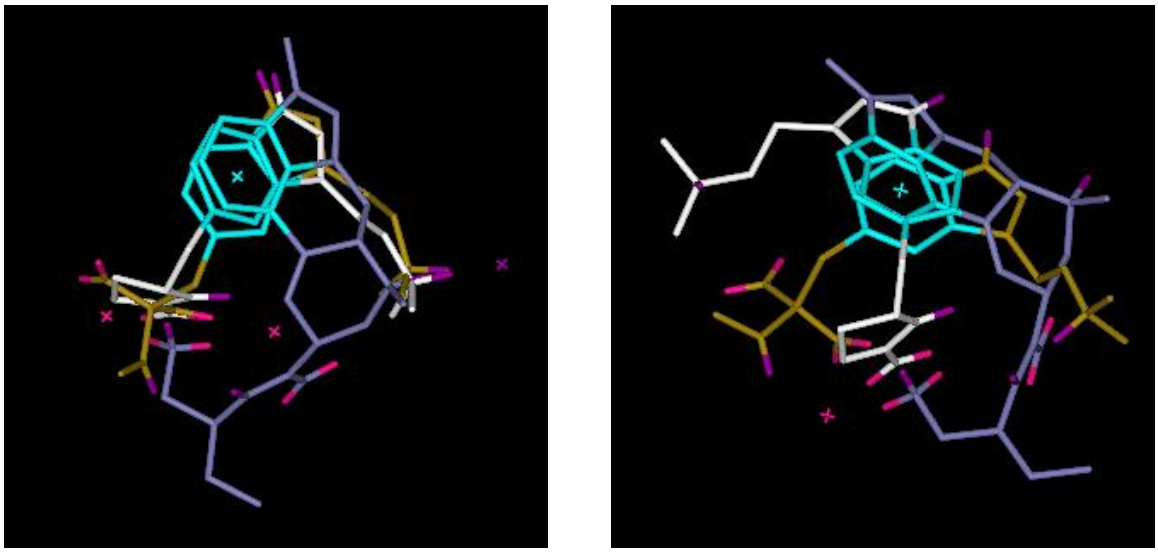

Figure 1.

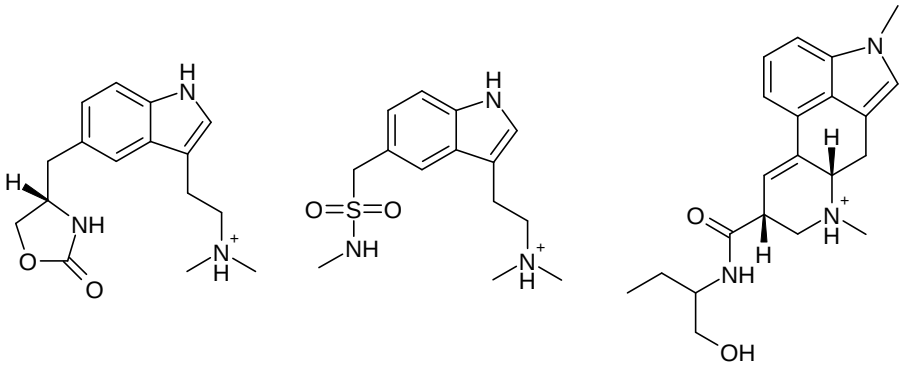

1 **2** **3**

Figure 2.

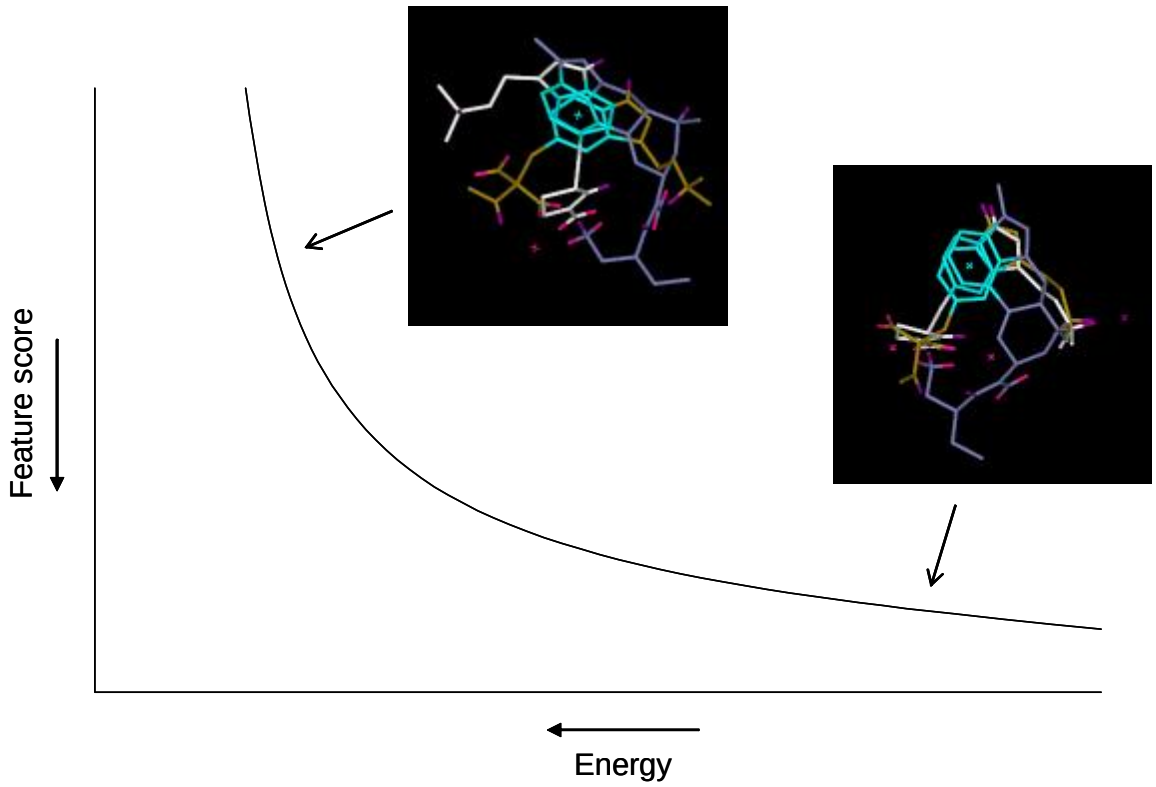

Figure 3.

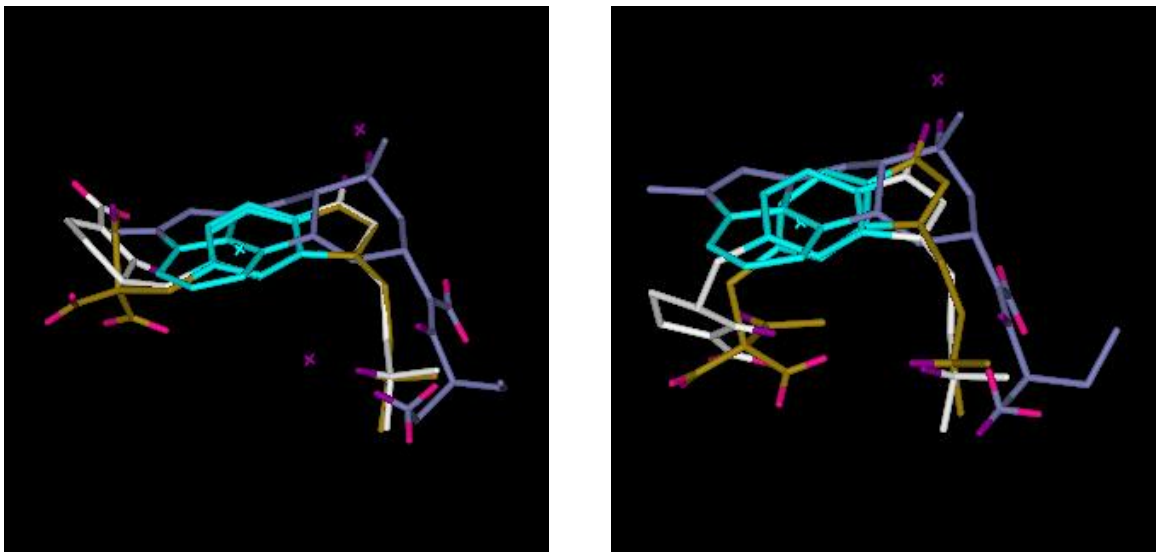

Figure 4.

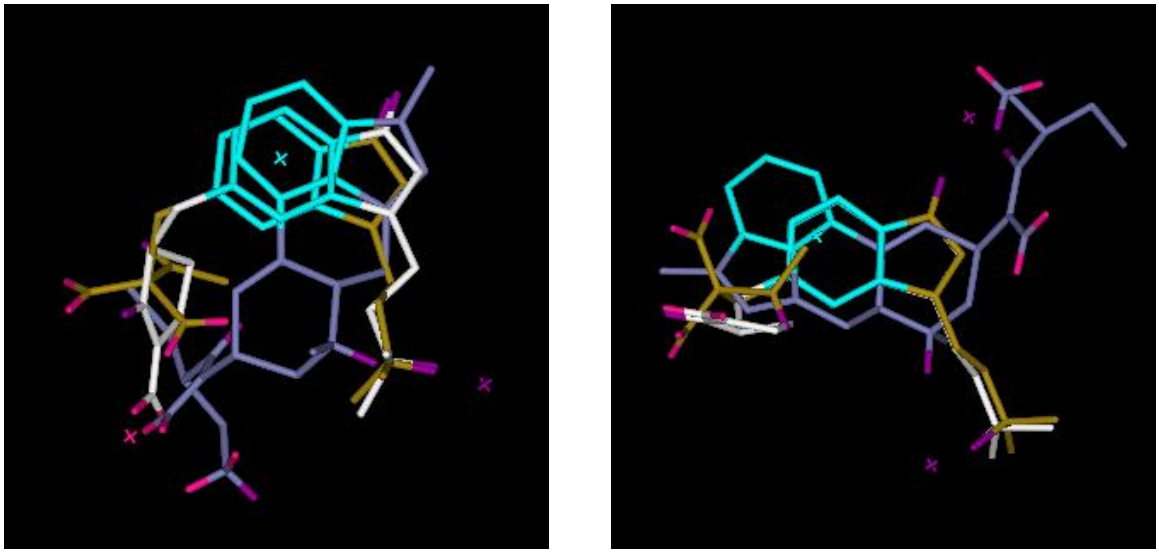

Figure 5.

1

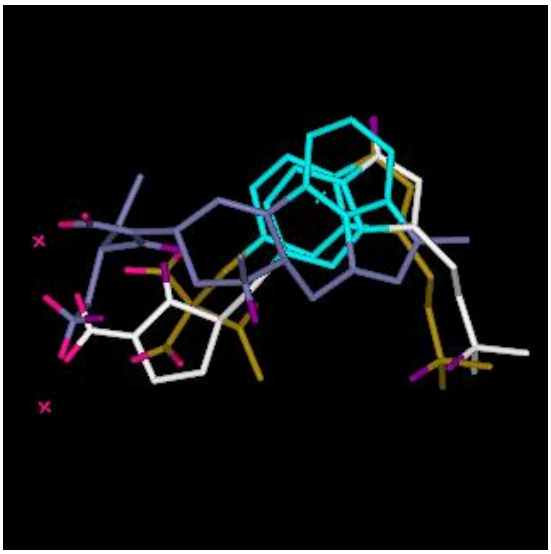

2

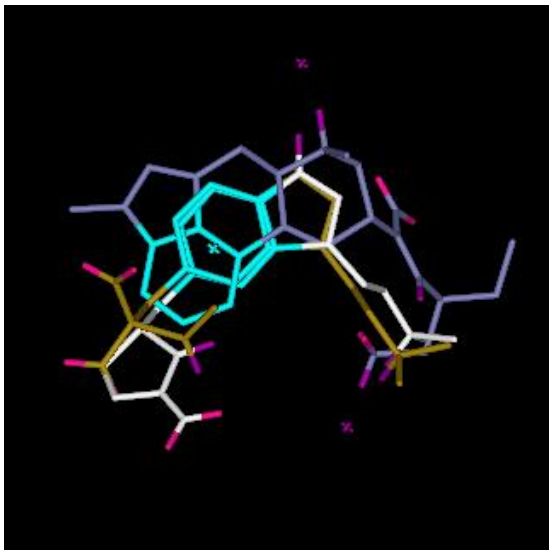

3

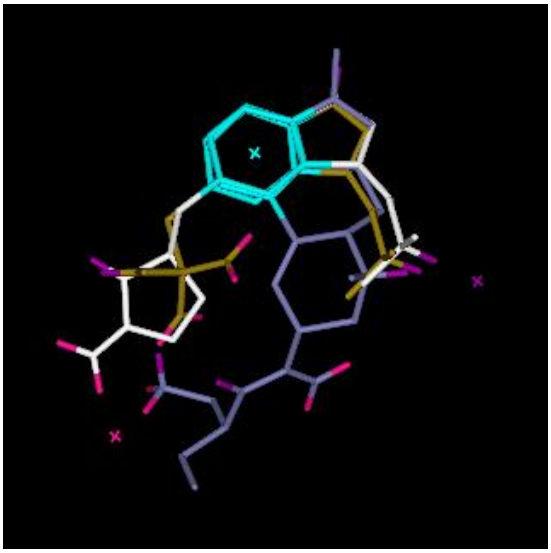

4

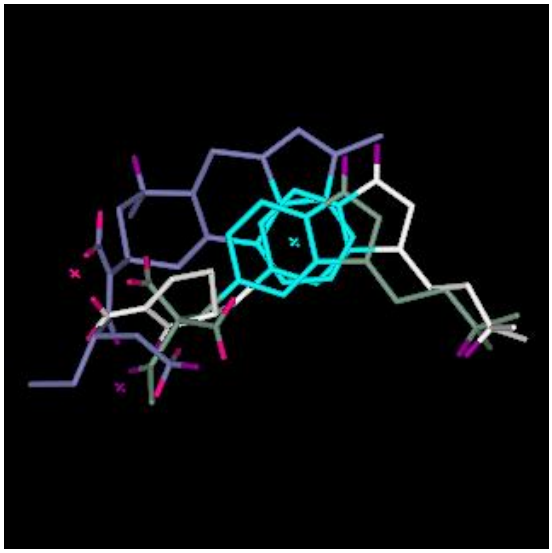

5

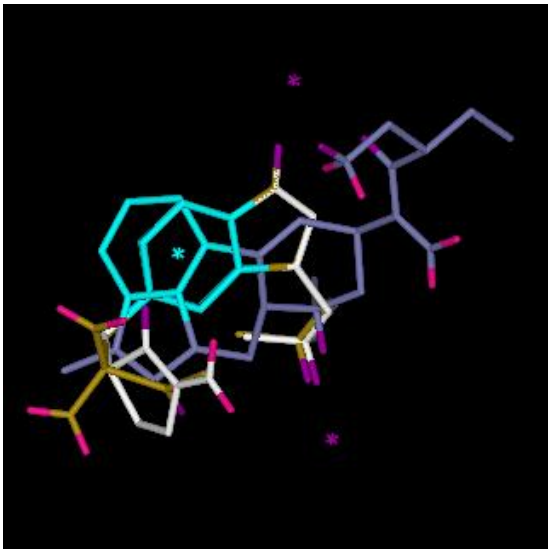

Figure 6.

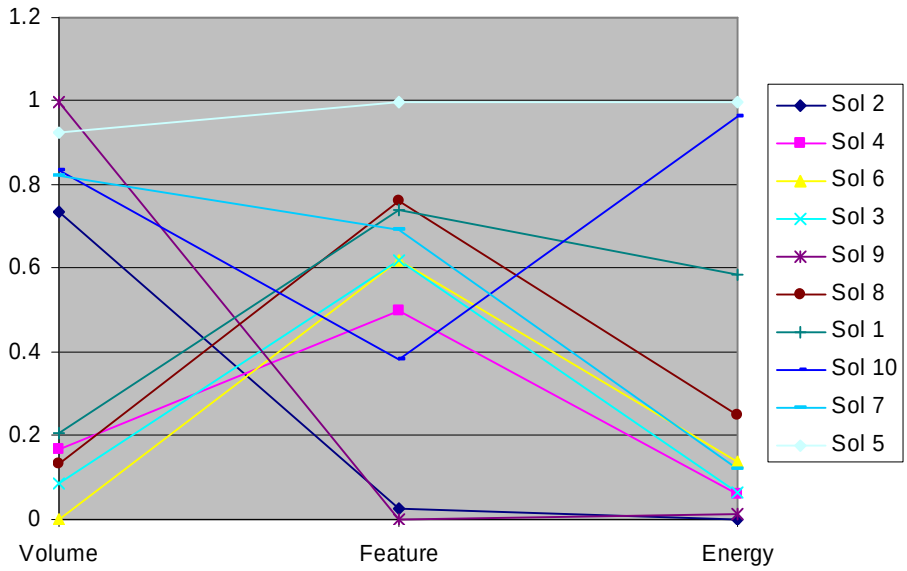

Figure 7a.

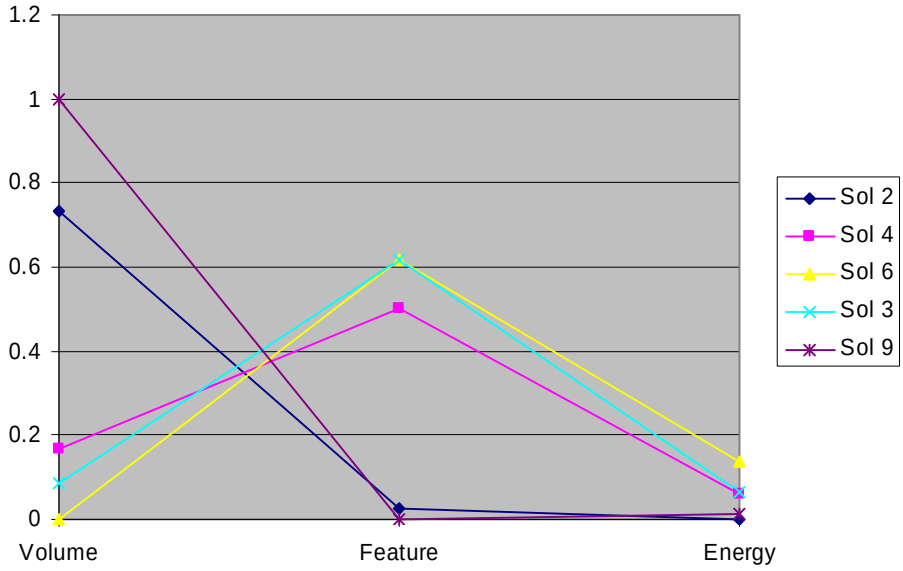

Figure 7b.

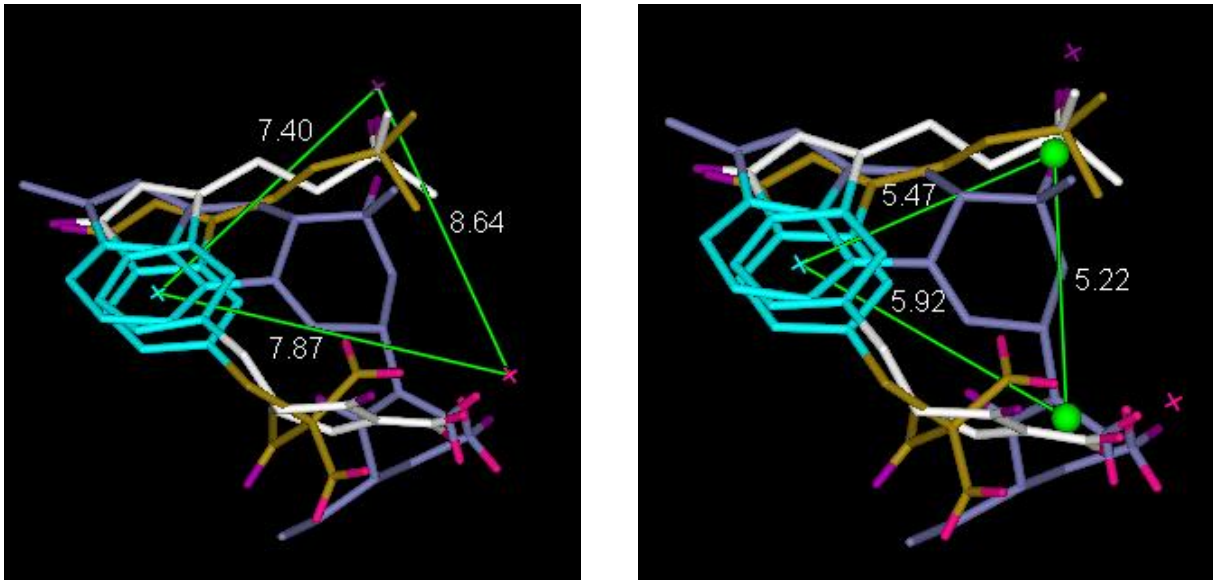

Figure 8.

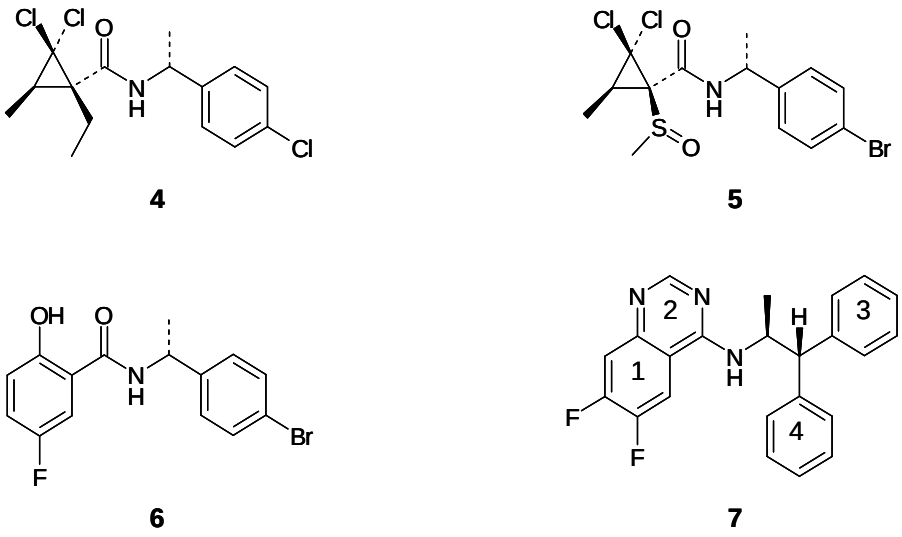

Figure 9.

(a) Ring 1

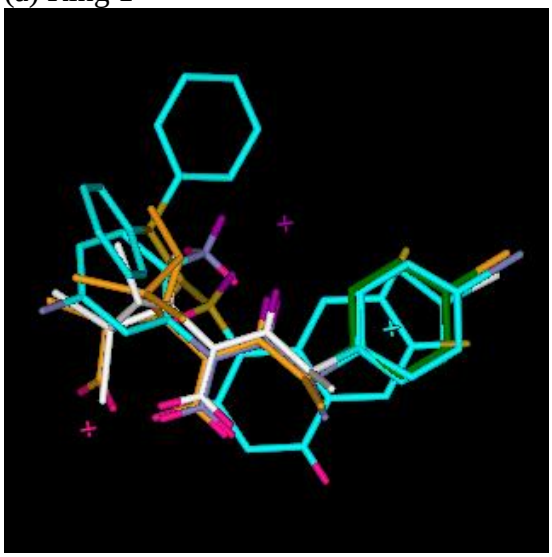

(b) Ring 2

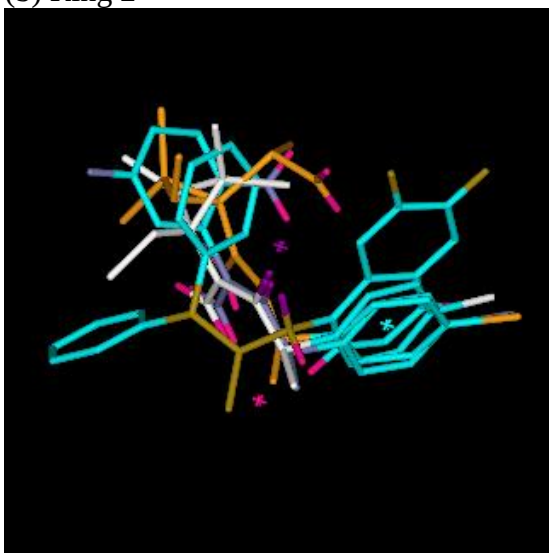

(c) Ring 3

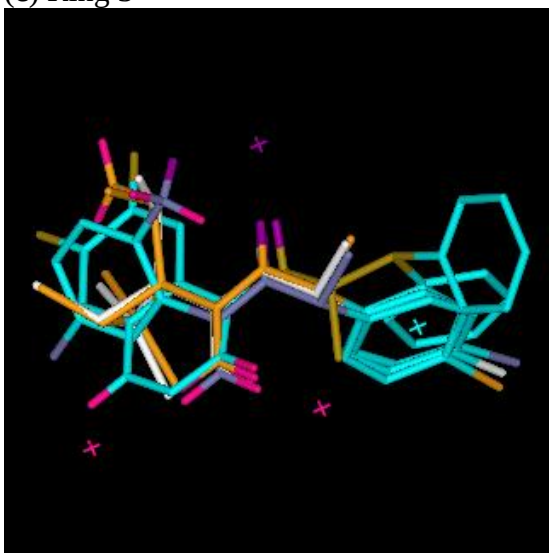

(d) Ring 4

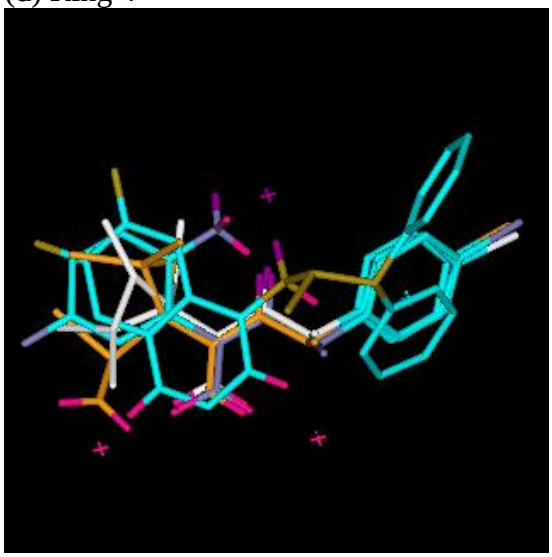

Figure 10.

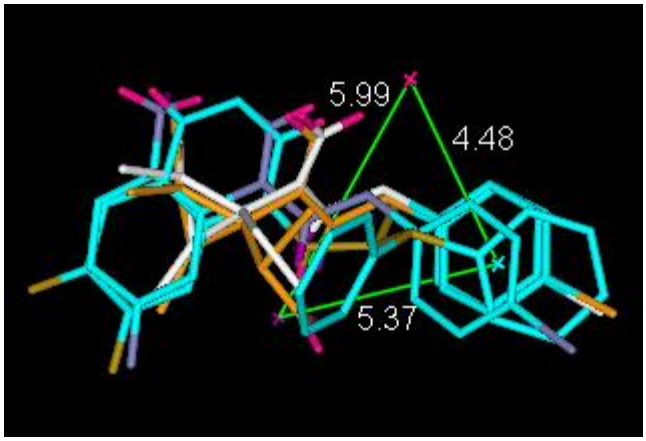

Figure 11.

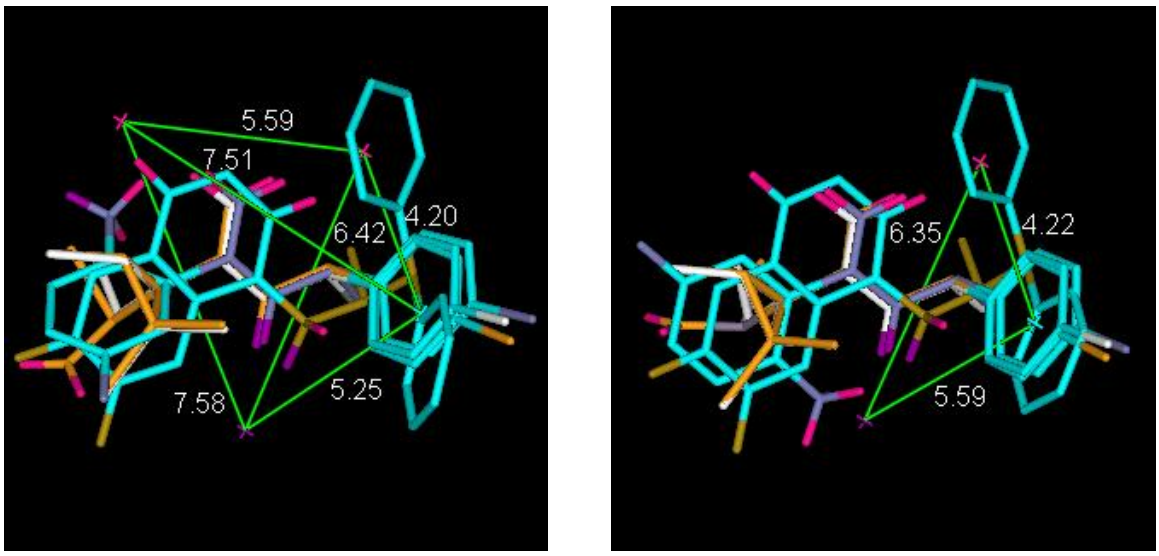

Figure 12.

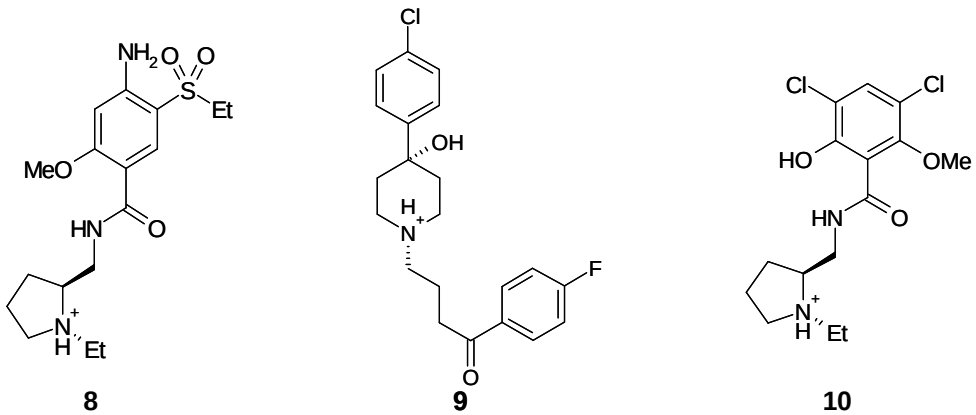

8 **9** **10**

Figure 13.

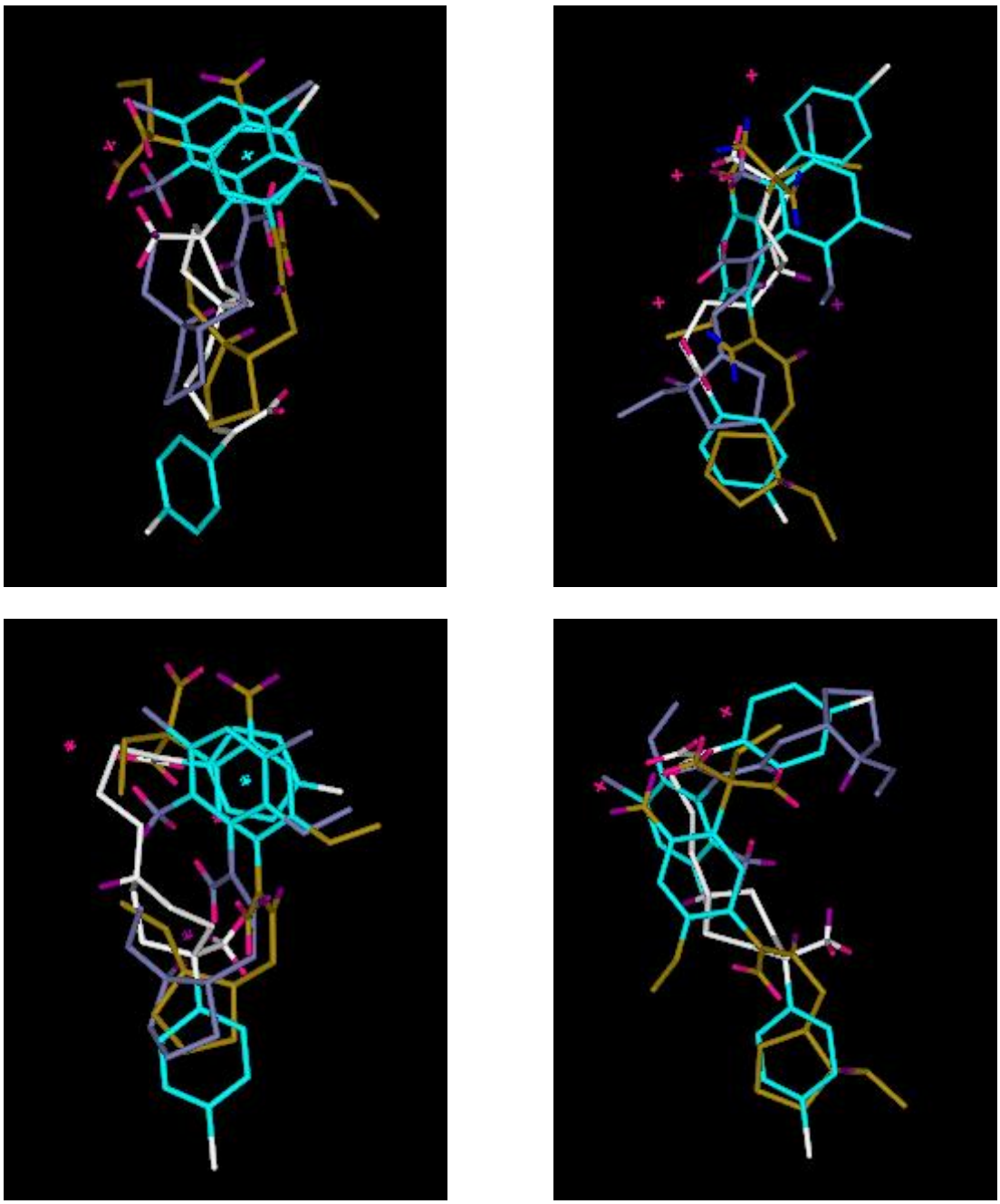

Figure 14. Alignments of dopamine D_2 antagonists.